Flow Evolution and Energy Loss Mechanism in Accidental Shutdown Process of a Large Submersible Mixed-Flow Pump System

B. Zhu[1, 2 †], W. Han[1, 2], Z. Tai[1, 2] and Y. Chen[3]

[1.]*School of Energy and Power Engineerning, University of Shanghai for Science and Technology, Shanghai 200093, China*
[2.]*Shanghai Key Laboratory of Multiphase Flow and Heat Transfer in Power Engineering, Shanghai 200093, China*
[3.]*Yangtze River Survey Planning and Design Research Co., LTD, Shanghai Branch, Shanghai 200439, China*

†*Corresponding Author Email: zbing@usst.edu.cn*

ABSTRACT

To investigate the accidental shutdown process for a large vertical and submersible mixed-flow pump unit in a drainage pumping station, a three-dimensional numerical method for this transition process was proposed according to the angular momentum balance theorem and rigid body rotation technology. We obtained the transient performance curves of the unit and the internal flow characteristics of the full flow channel. In addition, we also analyzed the energy loss distribution of the through-flow components during this progress based on the entropy production theory. The results show that the whole runaway process needs to go through four stages: the pump mode, the pump braking mode, the turbine mode, and the stable runaway mode. The pressure amplitude changes greatly in impeller and guide vanes, and the main fluctuation frequency is the blade frequency. There are higher harmonic frequencies in the dynamic rotor-stator interface. As the rotating speed increases in turbine mode, the negative pressure area near the impeller blade's trailing edge gradually increases. The entropy production method can be used to determine the location, intensity of energy loss during the transient process. If the rotating speed exceeds the allowed value in the runaway turbine mode, the interaction between blade tip vortex and hub vortex rope may cause loss of stability.

Keywords: Vertical and submersible mixed-flow pump; Accidental shutdown; Transition process; Entropy production; Computational fluid dynamics.

NOMENCLATURE

D	internal diameter		$\bar{p}$	average pressure of the monitoring point
f	turbulence fluctuation frequency			
i	current number of time step		Q	volume flowrates of the pump
J	rotational inertia moment		T	fluid temperature
k	turbulent kinetic energy		ρ	density
M_0	the driving torque of the motor		$u', v'\, w'$	components of fluctuation velocity
M_1	moment of water resistance		μ_t	turbulence viscosity
M_2	moment of wind resistance		μ	fluid viscosity
M_3	moment of bearing friction		μ_{eff}	effective viscosity
n	rotation speed		$\frac{d\omega}{dt}$	angular acceleration
n_s	specific speed of pump		Δt	specified time step size
p	instantaneous pressure		H	water head of the pump

1. INTRODUCTION

As the key device for energy conversion in water engineering infrastructure, pumps are mainly used for water supply and drainage, agricultural irrigation, flood control, environmental protection and river governance and etc. Hence, pumps play an important role in agricultural production and urban construction in modern society (Tsukamoto and

Ohashi 1982; Jin *et al.* 2011). Compared with other types of pumps, the vertical submersible pump is an integrated unit, which has the characteristics of compact and simple structures, convenient installation, and low operating noise (Jianjun and Hongquan 2018). Therefore, it is often applied in the situation with only limited available area of the pumping station, or without the requirement of construction of underground plant.

In recent years, with the continuous construction of new pumping stations, the stability issue has attracted researchers' attention. Accidents like the pumping station unit being shut down due to sudden power failure or mis-operation, and the intercept device on the discharge pipe refuses to operate, water back-flow may occur under the pressure difference between the upstream and downstream water levels of the pump unit. Thus, it may induce the pump reversely rotating into the turbine condition until it reaches the runaway state (Fu *et al.* 2020). In this process, the pump's performance, such as speed and flow rate, changes dramatically. This leads to serious flow separation, and other unstable flow phenomena in the device. Usually, this kind of flow phenomena is the cause of the system vibration and noise, and may further affect the unit's stability and safety (Xi *et al.* 2021). Therefore, it is of great importance to carry out the research on transition process to provide certain theoretical guidance for engineering design and practical operation.

Initially, the studies on pump transition procedures were focused on the pump's start-up process with experimental method (Feng *et al.* 2020). Tsukamoto and Ohashi (1982) conducted a rapid start-up test study on a centrifugal pump, and analyzed the transient external characteristics results. Wu *et al.* (2006) conducted an experimental study on the performance and pipeline resistance of centrifugal pump at quick start-up condition. The above-mentioned experimental tests require the pump to be accelerated till a runaway speed, which can easily excite the resonance of the machine. Hence, this sort of experimental operation usually involves huge risk of damaging the testing machine and it's motor (Trivedi *et al.* 2018). In general, the experimental study is of great cost and potential risk.

Other than the experimental study, many scholars have proposed some other methods such as the one-dimensional characteristic line method to calculate and analyze the transient flow behavior of the pump system. Thanapandi and Prasad (1995) studied the transient laws of running speed, flow rate and water head at the moment of start-up and shutdown of a centrifugal pump by using the line method. Xi *et al.* (2021); Wang *et al.* (2010) studied the one-dimensional transition process of the pump system, and discussed the closing law of the valve behind the pump and the optimization process of the air valve arrangement scheme. Kim *et al.* (2015) calculated the hydraulic transient process in a pump station after a power failure based on the characteristic line method, and applied numerical analyses of water hammer for a pump-pipeline system with an air chamber. Rezghi and Riasi (2016) conducted numerical research on sensitivity of hydraulic parameters for two parallel pump-turbine units under runaway condition based on Suter transform method. Rohani and Afshar (2010) proposed an implicit characteristic line method for effectively simulating the instantaneous flow caused by pump failure, which required less computation. Obviously, the characteristic method plays a pivotal role in the early analysis of the fluid transient flow process, but the method has limitations as it cannot accurately capture the detailed transient flow fields inside the system (Fu *et al.* 2020).

With the rapid development of computational simulation technology, numerical simulation has been widely used, more and more scholars have begun to use this technology to study the transition process of the pump units. Zhang *et al.* (2013) conducted simulation and experiment for a centrifugal pump shutdown process by establishing a closed pipeline system, and analyzed its transient characteristics and flow field evolution. Wang *et al.* (2022) carried out numerical simulation of a water turbine runaway process based on the CFX platform and developed Fortran programs. Fu *et al.* (2020) simulated the transient flow characteristics of pipeline pump during its outage runaway process based on VOF model in Fluent. Kan *et al.* (2022) carried out numerical simulation of an axial-flow pump model during the power failure process, and obtained the evolution features of rotational speed, flow rate, and torque, as well as the evolution process of the cross-sectional flow velocity field and the impeller blade surface pressure. Xi *et al.* (2021) explore the transient characteristics of the large-scale vertical siphon axial flow pumping station during the start-up and exhaust process with numerical simulation method, it shows that the flow separation phenomenon of the impeller channel of the pump device with the vacuum breaking valve closed is serious, the large-scale vortex in the guide vane blocks the flow channel, and the instantaneous impact on the blade surface is strong.

In general, it can be shown that the above-mentioned works on transient process are mainly focused on centrifugal pumps, pump turbines or axial flow pumps. It lacks the work about the accidental shutdown process for a large vertical submersible mixed flow pump unit. Hence, we aim to investigate the accidental shutdown process for a large vertical and submersible mixed-flow pump unit in a drainage pumping station. In this paper, a prototype vertical submersible mixed-flow pump unit for drainage pump station is selected. The real-time rotating speed of the pump unit is obtained by solving the angular momentum equation acting on the rotating part in ANSYS Fluent. Combined with the rigid body rotation technology, a three-dimensional transient numerical calculation method for transient process analysis can be established. By this way, we can obtain the performance parameters of the system and the evolution characteristics of the flow field. The research results provide some interesting suggestions for the design of large-scale vertical submersible mixed-flow pumping stations.

2. PHYSICAL MODEL AND DOMAIN DISCRETIZATION

2.1 Pump Parameters

A vertical submersible mixed-flow pump is selected as the research object. The designed volume flow rate for each pump is Q=11m³/s, the water head is H=6.9m, the rotating speed is n=210 rpm, specific speed of the pump is defined as $n_s = \frac{3.65n\sqrt{Q}}{H^{0.75}} = 597$, and the electrical power is 1250kW. More detailed parameters of the pump are listed in Table 1.

2.2 Mesh Sensitivity

The working condition with highest static head is selected to study the transition process, and the computing region is shown in Fig. 1. The flow components of the pumping station are mainly composed of four parts: inlet channel, impeller, guide vanes and the outlet channel. In addition, in order to improve the robustness of simulation, the extended inlet region and outlet region are respectively added to the whole computation domain.

High-quality mesh plays a key role in the stability and accuracy of the simulation. The designed three-dimensional model was imported into the professional mesh generation software ICEM-CFD. The structure meshes of impeller and guide vanes were performed in Turbo-Grid. As shown in Fig. 2, the boundary layer of blades is surrounded by O type topological structure to improve the mesh quality and resolution near the blades.

The grid number directly affects the accuracy of the calculation results. We chose four different amount of grid sets (0.97, 1.47, 3.43 and 5.12 million) of the prototype pump at the design points for three-dimensional unsteady calculations. Since the torque moment on the impeller is the key for shutdown transient calculation to determine the real-time rotating speed, we chose the impeller torque parameter as the target function for mesh sensitivity verification. As shown in Fig. 3, the torque moment of the impeller changes with the increase of grid

**Table 1 Design parameters of the submersible mixed-flow pump.**

Parameters	Unit	Value
Number of impeller blades	/	3
Number of guide vanes	/	7
Rotational inertia (J)	kg. m^2	2175
Diameter of impeller	mm	1870
Rotational speed (n_0)	rpm	210
Design flow rate (Q_0)	m^3·s^{-1}	11
Water head (H_0)	m	6.9
Electrical power	kW	1250
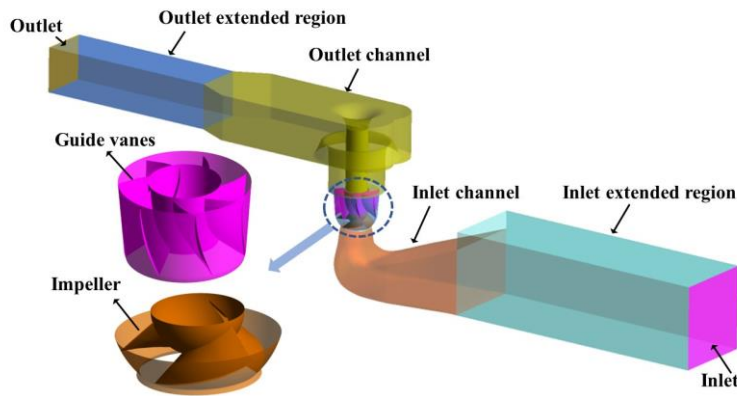
Fig. 1. Model of vertical submersible pump station unit.
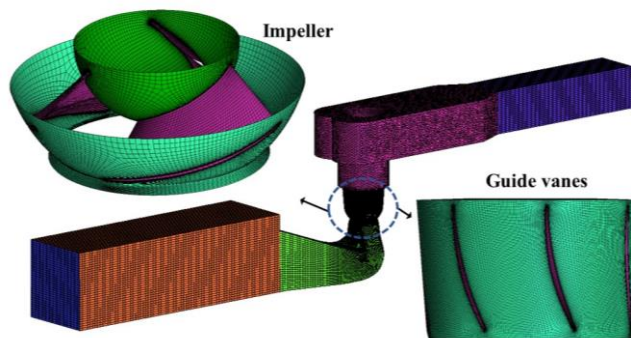
**Fig. 2. Mesh distribution of computation domain.**
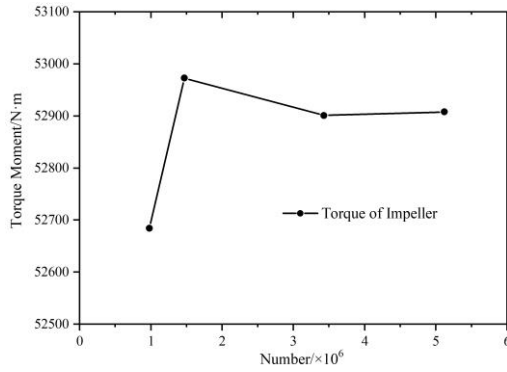
Fig. 3. Variation of impeller torque with mesh density change.

number. When the total grid amount exceeds 3.43 million, the impeller torque moment still remains almost unchanged. Therefore, we chose 3.43million grids for subsequent calculation.

2.3 Validation of the Numerical Method

To verify the reliability of the numerical calculation method, the corresponding model pump with D=320mm and n=1207 rpm is tested. The corresponding results are then converted to the prototype pump according to the principle of similarity. Meanwhile, the calculated results for the unsteady prototype pump case were compared with the test data, just as shown in Fig. 4. It can be shown that the numerical simulation results are slightly higher than the experimental result, which is due to
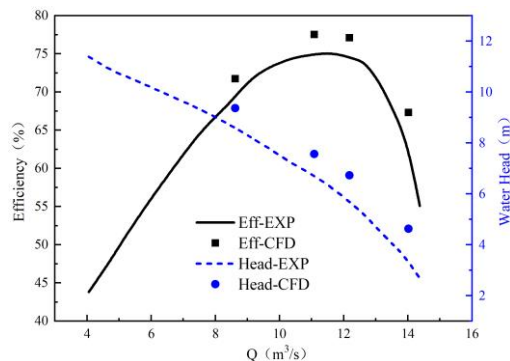
Fig. 4. Pump performance comparison between numerical results and experimental data.

the fact of ignoring the tip clearance, wall roughness and mechanical loss, and also the conversion error from model to prototype. However, the results of the numerical calculation and the trend of the pump performance are basically consistent with the test data within an acceptable error range.

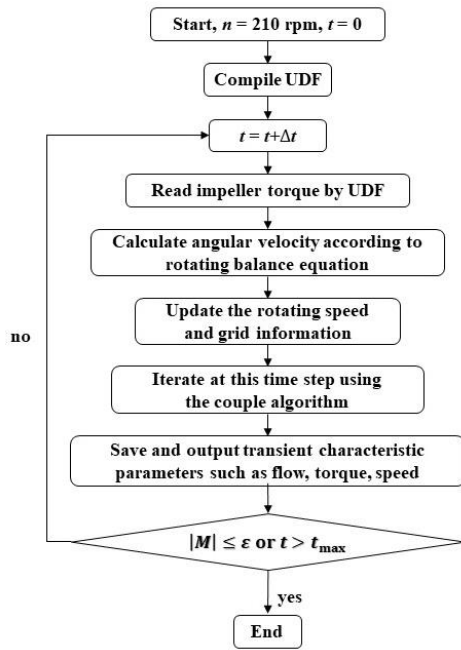## 3. TRANSITION NUMERICAL SIMULATION METHODOLOGY

3.1 Angular Momentum Equation

During the accidental shutdown progress of a pumping station, the impeller rotating speed follows the balance equation of angular momentum acting on the impeller (Feng *et al.* 2020), i.e. $J\frac{d\omega}{dt} = M_0 - M_1 - M_2 - M_3$. Where, J is the rotational inertia moment of the motion part, which is calculated as the value of 2175kg·m^2 according to the three-dimensional prototype geometry and material density; $\frac{d\omega}{dt}$ is the angular acceleration; M_0 is the electromagnetic torque of the motor, and it is zero during the runaway process; M_1 is the water resistance moment acting on the impeller by the water flow, which is calculated and updated at each time step according to the flow fields with a user defined function (UDF) in Fluent. M_2 is the moment of wind resistance, which is very small compared to the water resistance moment, so it can be ignored in this calculation. M_3 is the moment of bearing friction. It is neglected here for simplicity, but the calculations are subject to some error caused by the lack of the frictional moment for a real prototype unit. The rotating speed is updated by using $\omega_{i+1} = \omega_i + \frac{M_0 - M_1 - M_2 - M_3}{J} \times \Delta t$, i is the current time step number, and Δt is the specified time step size.

3.2 Simulation Method

The transient calculation for the pump shutdown process were conducted in the commercial software of ANSYS Fluent with the shear stress transport turbulence model (SST k-ω). The SST k-ω model has both the advantages of k-ε model and k-ω model, and can take into consideration the flow separation phenomenon under unfavorable pressure gradient conditions to some extent (Menter 1994, 2009; Mao *et al.* 2014). The method of whole domain with rigid body rotation was chosen to update the impeller location. The sliding mesh model at the interface was applied for the data transfer between rotating domain and stationary domain. The second-order scheme is adopted for the unsteady term, diffusion term and convection term. The discrete equations for pressure and velocity were solved discretely with coupling algorithm.

The boundary conditions for inlet and outlet are respectively set as the total pressure and static pressure according to the water level difference between the upstream and downstream of the pumping station. The time step is set as the time interval allowing the impeller rotating of one degree

```
┌─────────────────────────────┐
│  Start, n = 210 rpm, t = 0  │
└─────────────────────────────┘
              │
        ┌───────────┐
        │ Compile UDF │
        └───────────┘
              │
        ┌──────────┐
        │ t = t+Δt │
        └──────────┘
              │
   ┌──────────────────────────┐
   │ Read impeller torque by UDF │
   └──────────────────────────┘
              │
   ┌────────────────────────────────┐
   │ Calculate angular velocity according to │
   │      rotating balance equation          │
   └────────────────────────────────┘
              │
   ┌──────────────────────────┐
   │   Update the rotating speed    │
   │     and grid information        │
   └──────────────────────────┘
              │
   ┌──────────────────────────┐
   │   Iterate at this time step using │
   │      the couple algorithm         │
   └──────────────────────────┘
              │
   ┌────────────────────────────────────┐
   │ Save and output transient characteristic │
   │ parameters such as flow, torque, speed    │
   └────────────────────────────────────┘
              │
        ◇ |M| ≤ ε or t > t_max ◇
              │ yes
        ┌───────┐
        │  End  │
        └───────┘
```

Fig. 5. Algorithm schema for pump run-away transition simulation.

under pump working condition according to our previous experience. The standard of residual convergence in each time step is 10^{-5}, and the maximum number of internal iterations in each time step is 20.

During the numerical simulation, we first obtain an unsteady calculation result at a specified working condition of the pump station, and then we remove the driving moment to simulate the power cut-off progress. Thereafter, the rotational speed of the impeller changes in real time with the evolution of the flow field, and finally reaches the maximum reverse speed under a certain water level difference. Since the time for the unit entering the runaway condition is unknown in advance, the total simulation time should be set long enough during the calculation. The rotation speed, mass flow and moment of the impeller are monitored during this procedure, so as to determine the transition

characteristics. The basic simulation procedure is shown in Fig. 5.

4. RESULTS AND ANALYSIS

4.1 Characteristics of Performance Parameters

Figure 6 shows the transient variations of speed, flow rate, torque moment and axial force during the runaway process of power failure. In order to compare these values with those of the normal working conditions of the pump system, we have done the normalization of the dynamic parameters. The dynamic values that change with time are compared to the initial values. It can be seen that there exist four stages through the whole running away process: the pump mode, the pump braking mode, the turbine mode, and the stable runaway mode. Supposing the unit being disconnected from the power after 0.72s of stable pump operation, the unit is then no longer affected by the driving force of the motor and the impeller starts to decelerate under the action of water resistance torque until the speed drops to zero at about 2.86s. Then, the water resistance torque becomes the reverse driving torque, which makes the pump impeller accelerate in the reverse direction until the runaway speed under the specified static head level is reached. Besides, we also found that the variation trend of the impeller rotating speed is not synchronized with flow rate changing. This is mainly due to the fact that the water head provided by the impeller is balanced by the pressure difference of the outlet to inlet water level and the hydraulic loss through the entire pump flow passage when the impeller rotating speed is reduced. The performance curve demonstrated that although the pump impeller is rotating, the flow rate of the pump device is zero. With further decrease of the rotating speed, the work done by the impeller to the fluid is not enough to overcome the static pressure difference and hydraulic loss. At this moment, the water flow starts to reversely flow from the outlet to inlet, that is, the phenomenon of backflow occurs. At the time about 8.7s, the torque periodically oscillates around zero, and the rotating speed reaches the
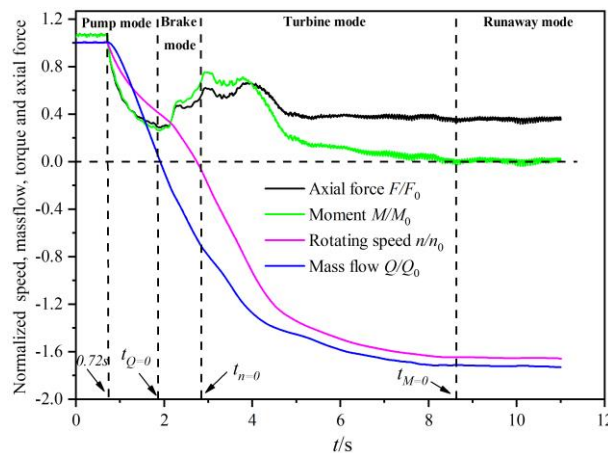
Fig. 6. Transient variation of the key dynamic parameters in pump runaway process.

maximum runaway speed of 347 rpm, which is about 1.65 times the rated speed. The direction of axial force does not change during the whole process of the pump being out of control, which is always in the same direction as the gravity. Hence, there is no possibility of the so-called ascension phenomenon.

4.2 Pressure Fluctuations

In the process of power failure, the change of the flow field of the pump unit leads to the change of the internal pressure. Thus, the different pressure monitoring points are selected at three typical sections, namely A, B and C, as shown in Fig. 7, indicating respectively the impeller inlet, impeller outlet and guide vane's outlet of the pump unit. Three monitoring points are arranged at span=0.1, 0.5, and 0.9 in each plane (A: $a_1 \sim a_3$, B: $b_1 \sim b_3$, C: $c_1 \sim c_3$). The pressure coefficient Cp is used to eliminate the effect of static pressure at each monitoring points,

which is defined as (Bejan 1996; Xi *et al.* 2021) $(C_p = (p - \bar{p})/0.5\rho u^2)$. Where, $\bar{p}$ is the average
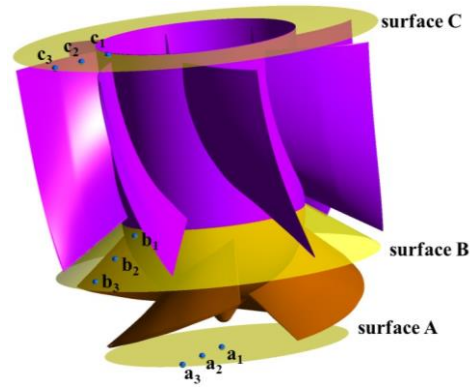

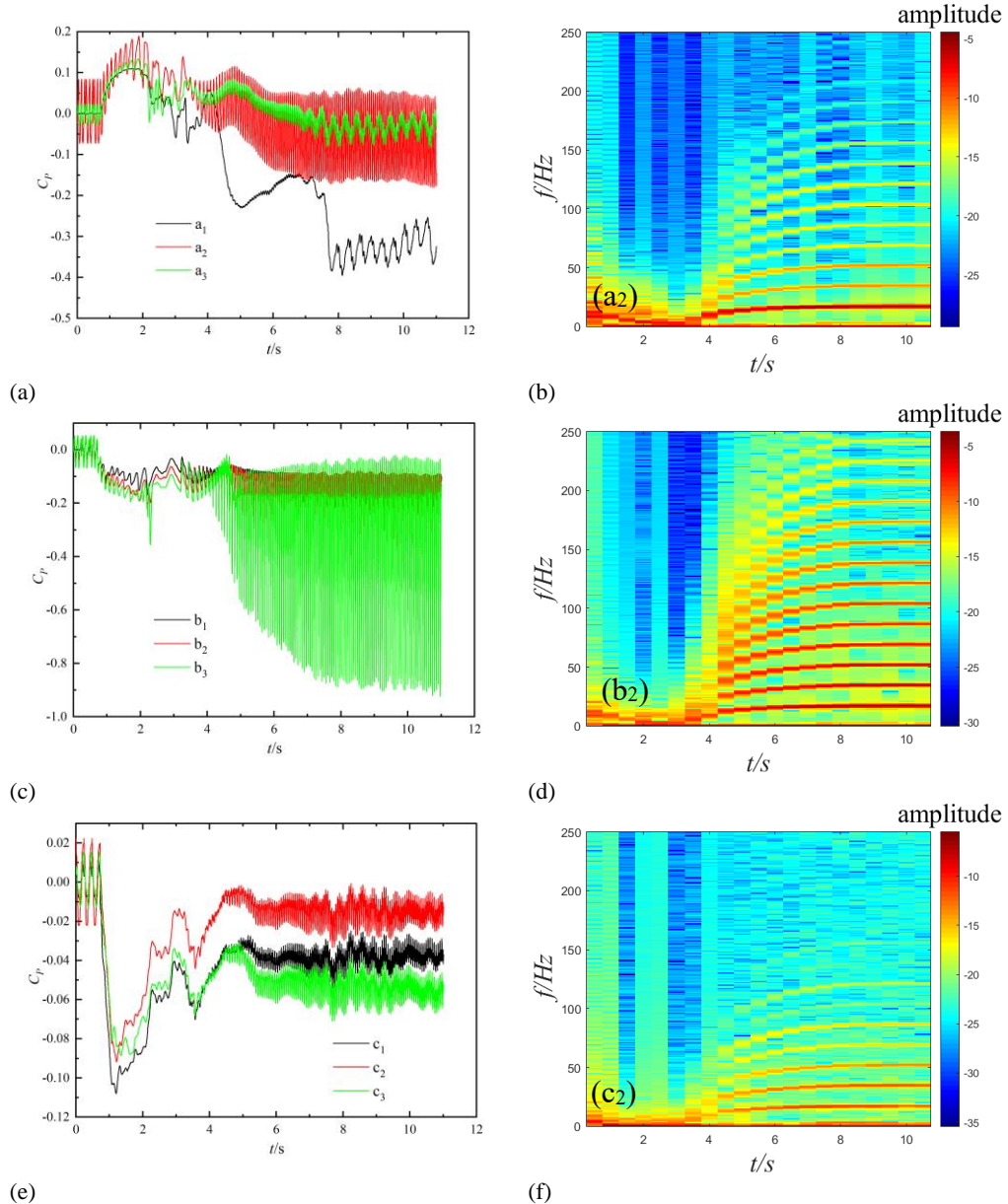**Fig. 7. Locations of monitoring points.**

Fig. 8. Pressure fluctuations of monitoring points.

pressure of the monitoring point when the pump is running at normal conditions, p is the instantaneous pressure during the transition process, ρ is the liquid density, u is the maximum blade tip speed at normal pump mode. To analyze the frequency changing characteristics of the pressure fluctuation in the pump runaway process, a short-time Fourier transform (STFT) was performed with a Hamming window function at point of a2, b2 and c2, respectively.

Figure 8 shows the time domain (a, c, e) and frequency domain (b, d, f) of the pressure fluctuations at different monitoring points during the transition process. It shows that, between the power-off to braking mode, the monitoring pressure on section A presents a completely opposite variation trend when comparing with section B and C. At section plane A, due to the sudden removal of the driving torque after the power failure, the water flow drives the impeller to do deceleration movement and the flow velocity also changes sharply. At this moment, the water flow in the inlet pipe section is subject to the flow inertia, which produces the water impact to the impeller. The formation of positive water hammer effect results in the pressure rise at the monitoring point until the system crosses over the pump mode. When the pump enters turbine operation mode, the water flow causes the impeller to perform reverse acceleration until it reaches a stable runaway speed. During this period, the static pressure at section A decreases and gradually tends to a stable state of periodic pulsation. The pressure at point a1 near the hub is significantly lower than the other two points at a2 and a3. This can be explained by the evolution of the vortex belt in the inlet flow channel shown in Fig. 15. The pressure in the central area of the inlet passage decreases when the pump unit starts to reverse. At section B, due to the negative water hammer effect, the pressure at the monitoring point drops. A low peak value appears at 2.3s, and there is a corresponding small peak value of force and torque. As the impeller reverses and enters the turbine mode, the pressure at the monitoring point gradually decreases, and the severity of the pressure pulsation is b3, b2 and b1 in turn. If we combine analysis from Fig. 10 and Fig. 11, we can find out that the above-mentioned phenomenon is due to the pump reversal and the low-pressure area begins to appear near the trailing edge. It is enhanced with the increase of reverse rotational speed, which is more obviously observed from the hub to the tip of the impeller. At section plane C, the pressure at the monitoring points drops immediately when the unit is powered off and reaches the minimum value at 1.2s. This is because the pump rotating speed decreases sharply once the pump's driving torque is released, resulting in the pump water head dropping sharply. As it enters the runaway operation condition, the monitoring pressure approximately keeps a stable periodic oscillation. From the frequency analysis of points a2, b2, and c2, we can find that the blade passing frequency is dominant and multiple frequencies can be captured on section plane B for the interaction between the rotor and stator.

4.3 Flow Fields

In this section, we chose some special moments during power failure to explore the evolution mechanism of flow field. The selected moments are respectively at t=0, *Q*=0, *n*=0 and *M*=0. Here, *M* = 0 means the net torque on the impeller reaches zero, and the pump reverses its rotating direction and reaches the maximum runaway speed. Fig. 9 shows the streamline and static pressure distribution in the meridian cross-section of the pump unit at the specific characteristic time.

As seen from the results, when the pump is at normal working condition, the streamline distribution in the meridian cross-section is relatively smooth, without obvious undesirable flow patterns such as backflow, and only a small amount of vortex exists in the outlet channel for the space diffuse and redirection. When the driving torque of the impeller disappears, the impeller keeps rotating in the forward direction because of the fluid inertia. At the same time, the rotating speed gradually decreases under the action of water resistance torque, and the unstable flow phenomena in the tunnel such as vortex begin to appear and gradually develop. When the flow rate is zero, there is obvious unstable turbulence in the inlet and outlet channels, especially in the outlet channel. After that, the unit enters the braking condition and the water flow in the reverse direction, while the pump is still in forward operation. During this process, the flow state changes rapidly until the rotating speed reaches zero, and the water flow in the outlet channel gradually becomes smooth, while more and more obvious swirl area in the inlet channel begins to appear.

Then, the impeller begins to reverse, and the unit enters the turbine operating condition. During this stage, the flow in the outlet channel is relatively smooth, and the flow in the inlet channel is still relatively smooth due to the reformation of the flow fields, but the flow pattern is still relatively turbulent until the unit reaches the stable flyaway condition. At this moment, there is always a large area of vortex backflow area in the inlet channel.

Figure 10 shows the pressure distribution on the impeller blade's pressure surface (PS) and suction surfaces (SS) at several typical times during the runaway process. It illustrates that most areas of pressure surface are positive pressure, and most areas of the suction surface are negative pressure at the initial moment of pump operation. After the unit is powered off, the pump starts to decelerate, and when the speed drops to zero, part of the kinetic energy is converted into pressure energy in this process, which results in the pressure on the suction side increases, and the overall distribution is basically equivalent with the pressure side. When the unit rotates inversely and enters the turbine operating condition, with the continuous increase of the impeller speed until it reaches the runaway operating condition, obvious negative low-pressure area begins to appear near the trailing edge (water inlet edge at this situation) and obvious high-pressure area begins to appear near the trailing edge. As the inverse rotating

(a) t=0

(b) $t_{Q=0}$=1.92s

(c) $t_{n=0}$=2.76s

(d) $t_{M=0}$=8.7s
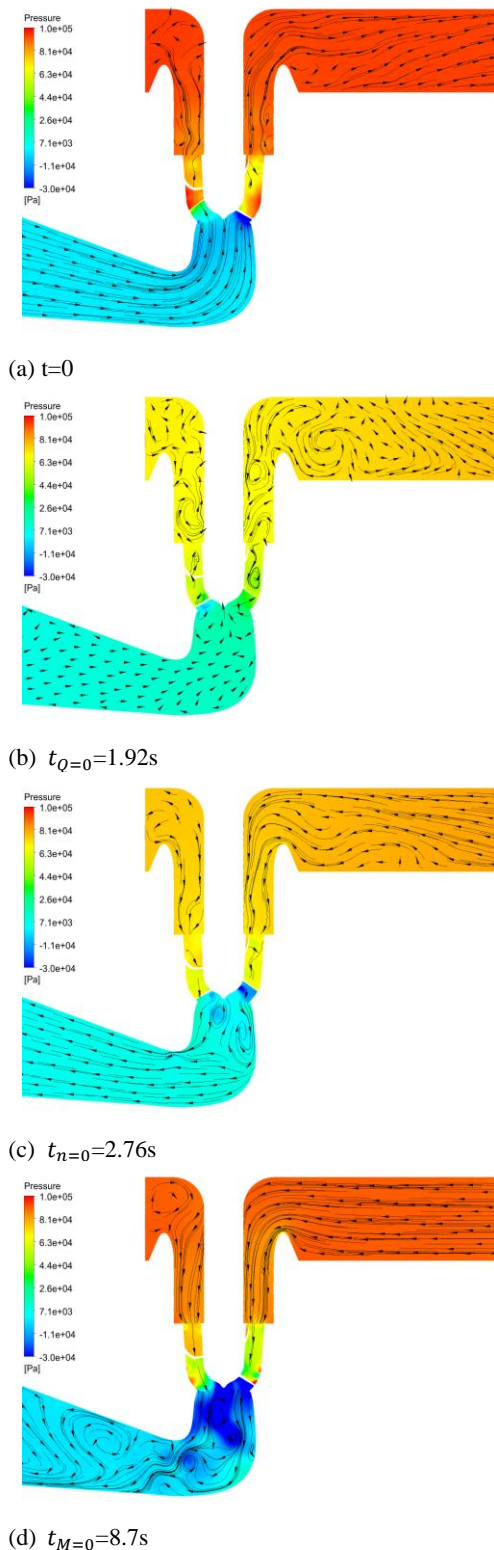
Fig. 9. Streamlines and static pressure distributions in meridian plane of pump.

speed increases during the runaway process, the water flow impacts the blade on the blade suction surface, which results in the serious flow detachment and generation of low-pressure area on the pressure side near the blade trailing edge. With the increase of rotating speed, the size of low-pressure area

(a) t=0s

(b) $t_{n=0}$=2.76s

(c) t=4.19s

(d) t=5.59s

(e) *t*=8.7s
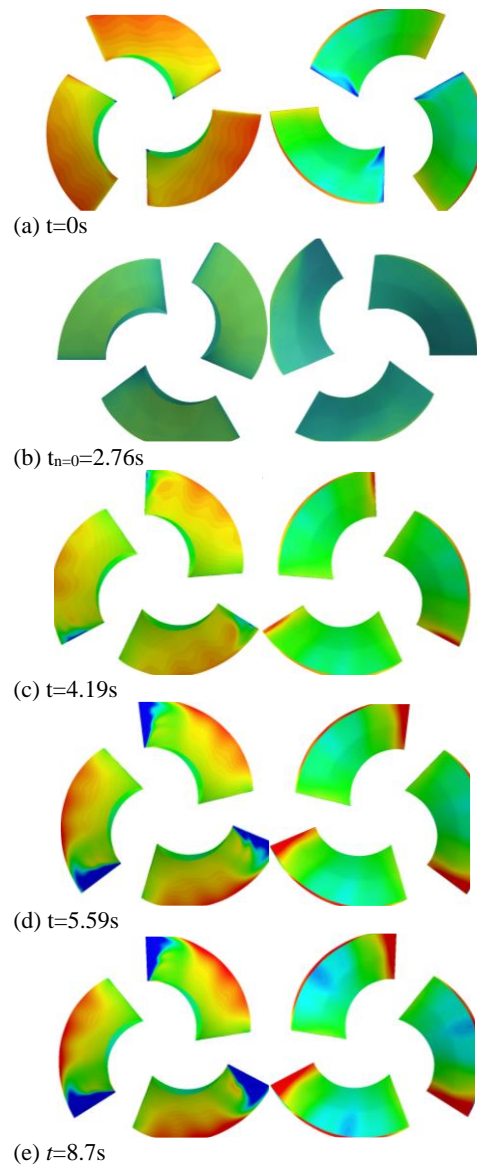
Fig. 10. Static pressure distribution on blade surface at different instants.

gradually increases. This increases the possibility of cavitation, flow detachment, and other unstable flow state. All these flow phenomena increase the operation risk of the pump unit.

To further analyze the flow evolution inside the impeller and guide vane during the whole runaway process, Fig. 11 shows the distribution of velocity and streamline at different spans and different moments. Because the maximum static water head between the inlet and outlet channels is selected for the current calculation, which is corresponding to off-design pump working condition, there is a certain vortex area near the guide hub, while it is stable in the impeller passage. When the power is shut off and the flow rate drops to zero, the kinetic energy provided by the impeller is not strong enough to overcome the gravity of the water flow itself, and it appears obvious reverse flow phenomenon in the guide vane section. As the rotating speed continues to decrease
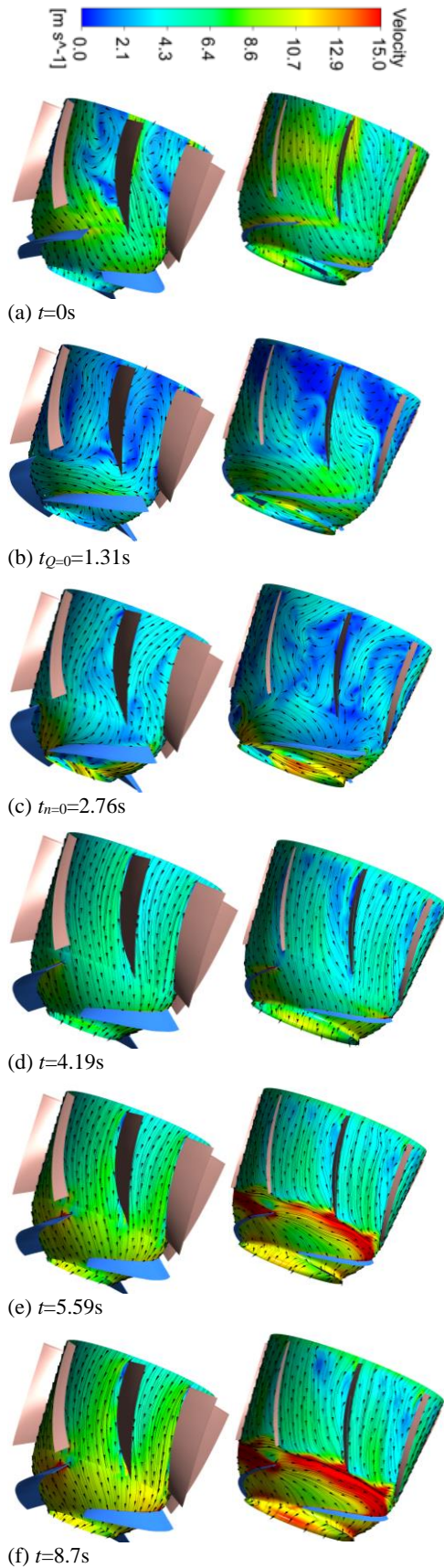
to zero, a global reverse flow area is shown both in the impeller and the guide vane. When pump enters the turbine mode, the pressure difference around the pressure side and the suction side, is greater at the blade tip area and more apparent with the increase of rotating speed.
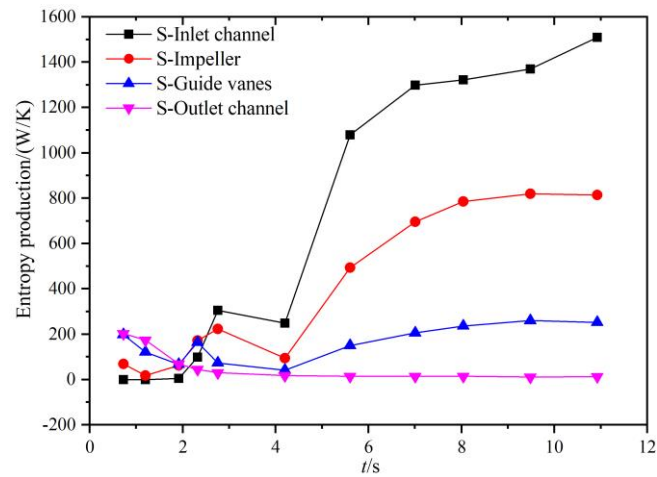
4.4 Distribution of Entropy Production

Entropy production is an unavoidable dissipative effect arising from the energy conversion process (Li *et al.* 2016). There are various unstable flows, such as vortex, flow separation, backflow, etc., in the process of accidental power failure of the pump device, and these turbulent flow patterns increase the loss and entropy production. In addition, fluid kinetic energy and pressure energy are converted into internal energy and dissipated energy, which also causes an increase of entropy production. Therefore, we can calculate the value of entropy production distribution in the whole flow field during the pump flyaway process, which can be applied to study and analysis the energy loss (Kock and Herwig 2004, 2005; Herwig and Kock 2006). Due to the large specific heat capacity of water, it can be supposed that the temperature is constant during this process, thus the entropy due to heat transfer can be ignored. Entropy production is generally expressed as the entropy generation rate (EGR). For turbulent flow, there are two main contribution sources of EGR, one is generated by the mean velocity, called the mean dissipation term, and the other is caused by the pulsating velocity, called the turbulent dissipation term (Bejan 1996).

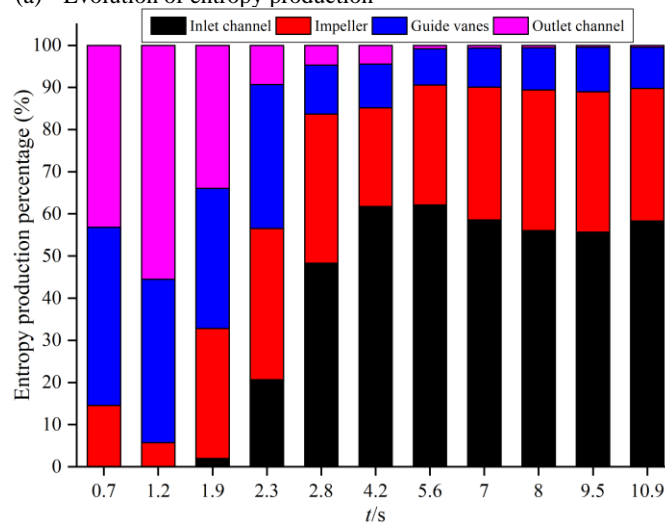The entropy yield (Zhou *et al.* 2022) due to average velocity is

$$\dot{S}_{\bar{D}}''' = \frac{\mu}{T} \sum_{i \neq j}^{3} \frac{1}{2} \left(\frac{\partial \bar{u}_i}{\partial x_j} + \frac{\partial \bar{u}_j}{\partial x_i} \right)^2 + 2 \frac{\mu}{T} \sum_{i=1}^{3} \left(\frac{\partial \bar{u}_i}{\partial x_i} \right)^2$$

$$\dot{S}_{D'}''' = \frac{\mu_{eff}}{T} \sum_{i \neq j}^{3} \frac{1}{2} \left(\frac{\partial u'_i}{\partial x_j} + \frac{\partial u'_j}{\partial x_i} \right)^2$$
$$+ 2 \frac{\mu_{eff}}{T} \sum_{i=1}^{3} \left(\frac{\partial u'_i}{\partial x_i} \right)^2$$

Where, $\bar{u}_i$ and u'_i, i= 1~3, are the average velocities and fluctuation velocities in the x, y, z directions. T is the fluid temperature, μ and μ_{eff} are the fluid dynamic viscosity and effective dynamic viscosity of the fluid, which can be calculated from $\mu_{eff} = \mu + \mu_t$, in which μ_t is the turbulent dynamic viscosity. Since the Reynolds averaged SST k-ω turbulence model is used for the current calculation, the entropy generated by the pulsation velocity can be approximated by $\dot{S}_{D'}''' = \beta \cdot \frac{\rho f k}{T}$. Where, $\beta = 0.09$, f is the turbulent pulsation frequency, k is the turbulent kinetic energy, ρ is the density. By integrating the above two parts of entropy in different regions, the distribution of entropy yields at each part can be obtained, namely the direct dissipation entropy yield $S_{\bar{D}} = \int_V \dot{S}_{\bar{D}}''' dV$ and the turbulent dissipation entropy yield $S_{D'} = \int_V \dot{S}_{D'}''' dV$. Therefore, the total entropy of the entire computational domain is obtained as $S = S_{\bar{D}} + S_{D'}$.

(a) *t*=0s

(b) $t_{Q=0}$=1.31s

(c) $t_{n=0}$=2.76s

(d) *t*=4.19s

(e) *t*=5.59s

(f) *t*=8.7s

Fig. 11. Velocity and streamline distributions at different instants (left: Span=0.5, right: Span=0.9).
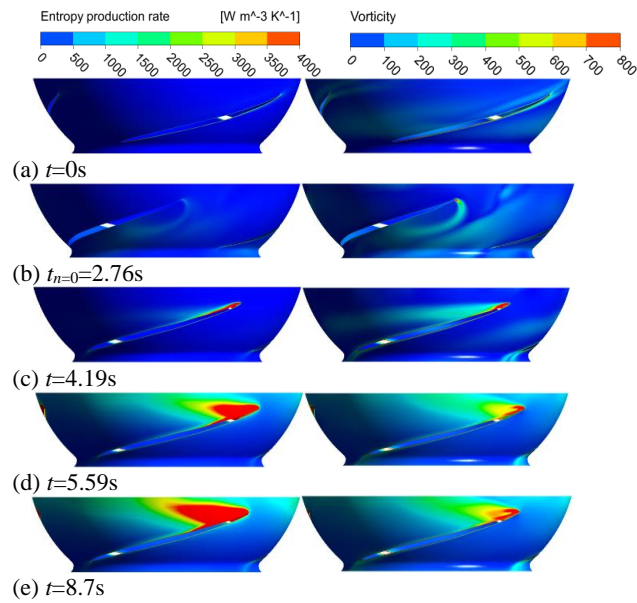
(a)   Evolution of entropy production

(b)   Entropy production percentage

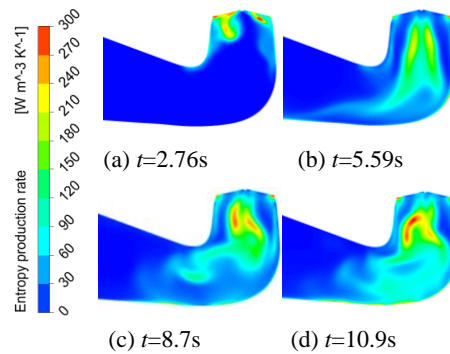**Fig. 12. Evolution of entropy production for different components.**

Figure12 shows the integrated entropy and its ratio of each component varies with time. It shows that the entropies obtained from the outflow channel and guide vanes are higher than that of the impeller and inlet channel at the initial pump normal working moment. When the flow rate of the unit reaches zero and starts to form the backflow phenomenon, the entropy production of the inlet channel starts to rise and exceeds those of the impeller and guide vanes at t≈2.5s, and the entropy production of the impeller exceeds that of the guide vanes after t=2.32s. As the unit enters the turbine mode and reaches the stable runaway state, the entropy production in the inlet channel and impeller gradually occupies the dominant position, and the largest entropy production component is the inlet channel, followed by the impeller, guide vanes and outlet channel, in which the entropy production in the inlet channel and impeller accounts for about 90% of the total entropy. It can also be seen from the Fig. 12 that the entropy production changes sharply during the period of t=1.9-5.6s. At this period, the unit is gradually operating from the braking mode to the turbine mode, and the flow field changes. Both the flow velocity and direction change dramatically, and

unstable flow phenomena such as turbulent eddies are prominent.

According to the above-mentioned change law of entropy production, we found that during the whole accident shutdown process, the entropy production of the inlet channel and impeller changes drastically. Besides, according to the previous flow field analysis, its change near the impeller rim is more obvious. Thus, we select the impeller section of span=0.9 and the X-Y section of the inlet channel to observe the entropy production distribution law and carry out in-depth analysis of its unstable flow. Fig. 13 shows the distributions of local entropy production rate and vortex at impeller span=0.9 at different moments during the accident shutdown process. It can be seen, as the unit enters the stable runaway state, the area with higher local entropy production rate is mainly concentrated in the area near the original trailing edge of the blade pressure side, which is corresponding to the inlet side in turbine mode. The distribution of local entropy production rate is basically the same as the distribution area of vortex, which indicates that the fluid is affected by strong vortex separation here.

Fig. 13. Entropy production rate (left) and vortex (right) distributions at Span=0.9.


Fig. 14. Evolution of entropy distribution in meridian plane near the elbow channel.

This causes the increase of hydraulic loss, which is consistent with the previous analysis. As seen in Fig. 14, the area of the high entropy production rate becomes gradually larger with the increasing rotating speed, and its distribution is very similar to that of the vortex at the inlet channel near the guide cone. All these further verify the reliability of the entropy production analysis, and it can be applied to describe the specific location, range, and intensity of the energy loss.

4.5 Vortex Rope Behavior

It can be seen from Fig. 15, when the reversing rotating speed of the unit is relatively low, three small swirling vortexes can be observed detaching from the impeller blade tip, and they interact with the elbow wall to form scattered small vortexes. As the turbine's rotating speed increases, the turbine's hub vortex begins to form, but it keeps relatively stable at the beginning, as shown in Fig. 15(b). Then, the hub vortex becomes stronger with more obvious spiral characteristics during approaching to the runaway
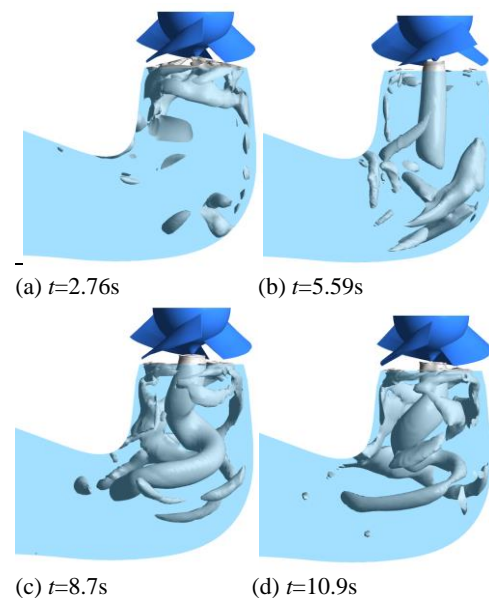
Fig. 15. Evolution of vortex rope in elbow channel.

condition. The hub vortex rope and its interaction with the blade tip vortex cause serious instability problems for the pump unit in the out-of-control state.

5. Conclusions

Based on the user-defined function scheme and rigid body rotation technology, we simulated the runaway transition process of a vertical submersible mixed-flow pump unit, and obtained several conclusions as following:

(1) The pump's whole running away process due to accident power off has four stages: the pump mode, the pump braking mode, the turbine mode, and the stable runaway mode. We should check carefully about the time period, the maximum flying away speed, and the axial force during the whole period. We also need to take some measures, such as breaking device, gate or valve adjustment, to control the potential risk or damage to the device.

(2) During the whole process, the pressure changes greatly and the main fluctuation frequency is related to the blade frequency. In the dynamic rotor-stator interface, it shows higher harmonic frequencies. As the rotating speed increases and approaches the runaway condition, the negative pressure area near the impeller blade's trailing edge gradually increases, which has a certain influence on the stable and safe operation of the pump device and its cavitation performance.

(3) There is an obvious correlation between the entropy production and the performance of the pumping unit. As the flow field evolves, the entropy production changes simultaneously. The energy loss is closely related to the unstable flow phenomena, such as flow separation, and vortex inside the flow field. The interaction between blade tip vortex and hub vortex rope leads high stability risk when the unit entering the flying-away turbine mode.

Reference

Bejan, A. (1996). Entropy generation minimization: The new thermodynamics of finite-size devices and finite-time processes. *Journal of Applied Physics* 79(12), 1191-1218.

Feng, J., Y. Zhang, G. Zhu, Y. Li, W. Li and X. Luo. (2020). Transition process characteristics of centrifugal pump with power-off based on entropy production theory. *Transactions of the Chinese Society of Agricultural Engineering* 36(4), 10-17.

Fu, S., Y. Zheng, K. Kan, H. Chen, X. Han, X. Liang, H. Liu and X. Tian. (2020). Numerical simulation and experimental study of transient characteristics in an axial flow pump during start-up. *Renewable Energy* 146(7), 1879-1887.

Herwig, H. and F. Kock. (2006). Direct and indirect methods of calculating entropy generation rates in turbulent convective heat transfer problems. *Heat and Mass Transfer* 43(18), 207-215.

Jianjun, Z. and Z. Hongquan. (2018). A review of experiments modeling of gas-liquid flow in electrical submersible pumps. *Energies* 11(1), 1-41.

Jin, J., C. Xiangping, D. Shengwen, N. Lina and H. Guanqiao. (2011). Protection with air-inlet-and-outlet valve from column separation in pumping system. In *International Conference on Materials for Renewable Energy & Environment*, shanghai,China.

Kan, K., Z. Xu, H. Chen, H. Xu, Y. Zheng, D. Zhou, A. Muhirwa and B. Maxime. (2022). Energy loss mechanisms of transition from pump mode to turbine mode of an axial-flow pump under bidirectional conditions. *Energy* 257(15), 124630.

Kim, S. G., K. B. Lee and K. Y. Kim (2015). Water hammer in the pump-rising pipeline system with an air chamber. *Journal of Hydrodynamics* 26(6), 960-964.

Kock, F. and H. Herwig. (2004). Local entropy production in turbulent shear flows: a high-Reynolds number model with wall functions. *International Journal of Heat and Mass Transfer* 47(10), 2205-2215.

Kock, F. and H. Herwig. (2005). Entropy production calculation for turbulent shear flows and their implementation in cfd codes. *International Journal of Heat and Fluid Flow* 26(4), 672-680.

Li, X., Z. Zhu, Y. Li and X. Chen. (2016). Experimental and numerical investigations of head-flow curve instability of a single-stage centrifugal pump with volute casing. *Proceedings of the Institution of Mechanical Engineers, Part A: Journal of Power and Energy* 230(7), 633-647.

Mao, J., S. Q. Yuan, J. Pei, J. F. Zhang and W. J. Wang. (2014). Applications of different turbulence models in simulations of a large annular volute-type pump with the diffuser. *IOP Conference Series: Earth and Environmental Science* 22(2), 1-8.

Menter, F. R. (1994). Two-equation eddy-viscosity turbulence models for engineering applications. *AIAA Journal* 32(8), 1598-1605.

Menter, F. R. (2009). Review of the shear-stress transport turbulence model experience from an industrial perspective. *International Journal of Computational Fluid Dynamics* 23(4), 305-316.

Rezghi, A. and A. Riasi. (2016). Sensitivity analysis of transient flow of two parallel pump-turbines operating at runaway. *Renewable Energy* 86(2), 611-622.

Rohani, M. and M. H. Afshar. (2010). Simulation of transient flow caused by pump failure: Point-Implicit Method of Characteristics. *Annals of Nuclear Energy* 37(12), 1742-1750.

Thanapandi, P. and R. B. N. Prasad. (1995). Centrifugal pump transient characteristics and analysis using the method of characteristics. *International Journal of Mechanical Sciences* 37(1), 77-89.

Trivedi, C., E. Agnalt and O. G. Dahlhaug. (2018). Experimental investigation of a francis turbine during exigent ramping and transition into total load rejection. *Journal of Hydraulic Engineering* 144(6), 1-16.

Tsukamoto, H. and H. Ohashi. (1982). Transient characteristics of a centrifugal pump during starting period. *Journal of Fluids Engineering* 104(1), 6-13.

Wang, F., M. Bai and R. Xiao. (2010). Analysis on hydraulic transients of pumping station with Flowmaster. *Paiguan Jixie Gongcheng Xuebao/Journal of Drainage and Irrigation Machinery Engineering* 28(2), 144-148.

Wang, P., X. Luo, J. Lu, J. Gao and Q. Cai. (2022). Influence of tubular turbine runaway for back pressure power generation on the stability of circulating cooling water system. *Water* 14(15), 2294.

Wu, D., L. Q. Wang and Z. Y. Hu. (2006). Experimental study on explicit performance of centrifugal pump during rapid starting period. *Journal of Engineering Thermophysics* 27(1), 68-70.

Xi, S., Z. Desheng, X. Bin, S. Weidong and B. P. M. van Esch. (2021). Experimental and numerical investigation on the effect of tip leakage vortex induced cavitating flow on pressure fluctuation in an axial flow pump. *Renewable Energy* 163(1), 1195-1209.

Zhang, Y., Z. Zhu, Y. Jin, B. Cui, Y. Li and H. Dou. (2013). Experimental study on a centrifugal pump with an open impeller during startup period. *Journal of Thermal Science* 22(1), 1-6.

Zhou, L., J. Hang, L. Bai, Z. Krzemianowski, M. A. El-Emam, E. Yasser and R. Agarwal. (2022). Application of entropy production theory for energy losses and other investigation in pumps and turbines: A review. *Applied Energy* 318(4), 1-21.